

## High frequency gyrokinetic particle simulation

R. A. Kolesnikov, W. W. Lee, H. Qin, and E. Startsev

*Plasma Physics Laboratory, Princeton University, P.O. Box 451, Princeton, New Jersey 08543, USA*

(Received 6 February 2007; accepted 30 May 2007; published online 13 July 2007)

The gyrokinetic approach for arbitrary frequency dynamics in magnetized plasmas is explored, using the gyrocenter-gauge kinetic theory. Contrary to low-frequency gyrokinetics, which views each particle as a rigid charged ring, arbitrary frequency response of a particle is described by a quickly changing Kruskal ring. This approach allows the separation of gyrocenter and gyrophase responses and thus allows for, in many situations, larger time steps for the gyrocenter push than for the gyrophase push. The gyrophase response which determines the shape of Kruskal rings can be described by a Fourier series in gyrophase for some problems, thus allowing control over the cyclotron harmonics at which the plasma responds. A computational algorithm for particle-in-cell simulation based on this concept has been developed. An example of the ion Bernstein wave is used to illustrate its numerical properties, and comparison with a direct Lorentz-force approach is presented. © 2007 American Institute of Physics. [DOI: [10.1063/1.2751600](https://doi.org/10.1063/1.2751600)]

### I. INTRODUCTION

The importance of gyrokinetic theory<sup>1-4</sup> for plasmas in a strong magnetic field has been widely appreciated. By removing the high frequency dynamics associated with fast gyromotion from the original Vlasov-Maxwell kinetic system, the gyrokinetic formalism yields a system of equations for describing low frequency ( $\omega \ll \Omega$ , where  $\Omega$  is the cyclotron frequency) and long wavelength phenomena in plasmas. However, the physics associated with the omitted high frequency part may be important. Particularly, in fusion plasmas, waves in both ion and electron cyclotron frequency ranges are used for plasma heating near resonance layers. In this paper we present a computational algorithm, which is an alternative to direct 6D Lorentz-force simulation<sup>5</sup> and which allows one to study arbitrary frequency dynamics of plasmas within the gyrokinetic framework. Here, for illustrative purposes, we only address the electrostatic case and leave the generalization to electromagnetic systems to future publications.

The high frequency gyrokinetic approach we discuss in this paper is based on the gyrocenter-gauge kinetic theory, developed by Qin *et al.*<sup>6,7</sup> in the limit of particle gyroradius much smaller than the scale length of the ambient magnetic field,  $\rho/L_B \ll 1$ . The gyrokinetic formalism transforms the Vlasov-Maxwell system in the 6D particle coordinate system  $\mathbf{z}=(\mathbf{x}, \mathbf{v})$  to a new 6D gyrocenter system  $\bar{\mathbf{Z}}=(\bar{\mathbf{X}}, \bar{U}, \bar{\mu}, \bar{\xi})$ . Here,  $\bar{\mathbf{X}}$  and  $\bar{U}$  are the location and parallel velocity of the particle gyrocenter,  $\bar{\mu}$  is the magnetic moment and  $\bar{\xi}$  is the gyrophase angle. While  $f(\mathbf{x}, \mathbf{v}, t)$  is the distribution function in the old particle coordinates,  $f(\bar{\mathbf{Z}}, t)$  is the distribution function in the new coordinates, where the parallel (gyrocenter) and the perpendicular (gyrophase) dynamics are decoupled. A similar approach was used by Lee *et al.*<sup>8</sup> for treatment of arbitrary frequency linear waves.

One of the advantages of an algorithm based on the gyrokinetic formulation is that it could be suitable for implementation into existing sophisticated gyrokinetic particle

codes<sup>9</sup> developed to study low frequency turbulence phenomena in general geometry. The motion of gyrocenters, which is slow compared to the gyrophase dynamics, may be treated with larger time steps. This separation of (gyrocenter and gyrophase) motions in the gyrokinetics, which results in significant saving in computer time, is not possible in Lorentz-force simulation. Contrary to low frequency gyrokinetics, which views each particle as a rigid charged ring,<sup>10</sup> we will show that, arbitrary frequency gyrokinetics describes each particle by a Kruskal ring.<sup>11,12</sup> Another advantage offered by the decoupling of motions introduced by the gyrokinetic approach is that it allows one to remove the explicit dependence on the gyrophase coordinate from the kinetic system. By doing this, one can reformulate the original 6D system in terms of five gyrocenter variables (5D), with the gyrophase dynamics represented by a set of equations for a finite number of harmonics kept. For certain situations computation of lower dimensional systems requires solving fewer differential equations and needs fewer simulation particles to achieve desired resolution in phase space, which results in further saving of computing time. Compared to 6D Lorentz-force codes, the high frequency gyrokinetic algorithms offer more computationally efficient and flexible approaches which may be useful for simulation of large systems (like global simulation of fusion plasmas in tokamak geometry<sup>9</sup>).

We believe that our new approach may be especially useful for computational study of the dynamics of propagation, conversion and absorption of radio frequency waves<sup>13-15</sup> in tokamak plasmas. Similar to a Lorentz-force simulation, the high frequency gyrokinetic algorithm allows a completely self-consistent simulation. Also, it can describe both linear and nonlinear heating dynamics based on first principle physics without extra assumptions about the quasi-linear nature of the heating mechanism.

This paper is organized as follows: In Sec. II we briefly review the gyrocenter gauge kinetic theory, which underlies our high frequency gyrokinetic system of equations. The 6D

algorithm based on this system is described in Sec. III. In Sec. IV we transform the explicit dependence on the gyrophase variable into equations for individual harmonics. This results in the 5D algorithm. The conclusions and future work are presented in Sec. V.

## II. HIGH FREQUENCY GYROKINETIC FORMALISM

The idea of the gyrokinetics is to identify a certain sequence of transformations<sup>6,7</sup> from the original particle coordinates  $\mathbf{z}$  to a new gyrocenter coordinate system  $\bar{\mathbf{Z}}$

$$\bar{\mathbf{Z}} = \mathbf{T}_{\text{gyro}} \mathbf{T}_{\text{guiding}} \mathbf{z}. \quad (1)$$

Here  $\mathbf{T}_{\text{guiding}}$  and  $\mathbf{T}_{\text{gyro}}$  stand for guiding center and gyrocenter transformations accordingly. One needs to make sure that the original kinetic equation for the distribution function  $f(\mathbf{x}, \mathbf{v}, t)$  in particle coordinates

$$\left( \frac{\partial}{\partial t} + \dot{\mathbf{x}} \cdot \frac{\partial}{\partial \mathbf{x}} + \dot{\mathbf{v}} \cdot \frac{\partial}{\partial \mathbf{v}} \right) f = 0 \quad (2)$$

transforms to a system of decoupled equations for the slow gyrophase-independent part of the distribution function  $F(\bar{\mathbf{Z}}, t) = F(\bar{\mathbf{X}}, \bar{U}, \bar{\mu}, t) \doteq \langle f(\bar{\mathbf{Z}}, t) \rangle$  and gauge function which contains all fast gyrophase dynamics. Here, the notation for a gyrophase-averaged quantity is introduced by

$$\langle a \rangle(\bar{\mathbf{X}}, \bar{U}, \bar{\mu}) \doteq (2\pi)^{-1} \int_0^{2\pi} a(\bar{\mathbf{Z}}) d\bar{\xi}, \quad (3)$$

$F(\bar{\mathbf{X}}, \bar{U}, \bar{\mu}, t)$  describes the evolution of the gyrocenter (parallel) dynamics according to

$$\frac{dF}{dt} \doteq \left( \frac{\partial}{\partial t} + \dot{\bar{\mathbf{X}}} \cdot \frac{\partial}{\partial \bar{\mathbf{X}}} + \dot{\bar{U}} \frac{\partial}{\partial \bar{U}} \right) F = 0. \quad (4)$$

The relation between different distribution functions is given by

$$f = \mathbf{T}_{\text{gyro}}^* \mathbf{T}_{\text{guiding}}^* F, \quad (5)$$

where  $\mathbf{T}_{\text{guiding}}^*$  and  $\mathbf{T}_{\text{gyro}}^*$  are pullback transformations, which transform the perturbed distribution functions between particles and guiding center, and guiding center and gyrocenter coordinates accordingly.

The near identity transformation

$$\mathbf{T}_{\text{gyro}}^* = \mathbf{1} + \delta\mathbf{T}(S(\bar{\mathbf{Z}}, t)) \quad (6)$$

depends on a special gauge<sup>6</sup> function  $S(\bar{\mathbf{Z}}, t)$ , which contains fast gyrophase (perpendicular) part of the dynamics. For an electrostatic system

$$\delta\mathbf{T}F(\bar{\mathbf{Z}}, t) = F(\bar{\mathbf{Z}}, t) \hat{\mathbf{Q}}_{\mathbf{T}} S(\bar{\mathbf{Z}}, t), \quad (7)$$

where

$$\begin{aligned} \hat{\mathbf{Q}}_{\mathbf{T}} \doteq & \frac{q}{mc} \frac{\partial \ln F}{\partial \bar{\mu}} \frac{\partial}{\partial \bar{\xi}} + \frac{1}{m} \frac{\partial \ln F}{\partial \bar{U}} \hat{\mathbf{b}} \cdot \frac{\partial}{\partial \bar{\mathbf{X}}} \\ & - \frac{1}{\Omega(\bar{\mathbf{X}})m} \frac{\partial \ln F}{\partial \bar{\mathbf{X}}} \cdot \hat{\mathbf{b}} \times \frac{\partial}{\partial \bar{\mathbf{X}}}. \end{aligned} \quad (8)$$

For an electrostatic system (and  $e\Phi/T \ll 1$ ), the gauge function  $S(\bar{\mathbf{Z}}, t)$  evolves according to

$$\dot{S} \doteq \left( \frac{d}{dt} + \Omega(\bar{\mathbf{X}}) \frac{\partial}{\partial \bar{\xi}} \right) S = q\tilde{\Phi}(\bar{\mathbf{X}} + \boldsymbol{\rho}, t), \quad (9)$$

where  $\tilde{a} \doteq a - \langle a \rangle$ . The new coordinate system  $\bar{\mathbf{Z}}$  makes sure that the gyrophase dependence is completely contained in Eq. (9). This allows transformation of explicit gyrophase dependence in Eq. (9) into a set of equations for individual harmonics. A 5D algorithm based on this transformation is presented in Sec. IV.

An appropriate conserved adiabatic invariant  $\bar{\mu}$  is obtained by expanding up to the first order term in the smallness parameter  $\rho/L_B \ll 1$ , and is given by

$$\bar{\mu} = \frac{mv_{\perp}^2}{2B(\bar{\mathbf{X}})} + \hat{\mathbf{Q}}_{\xi} S, \quad \hat{\mathbf{Q}}_{\xi} \doteq \frac{q}{mc} \frac{\partial}{\partial \bar{\xi}}. \quad (10)$$

The quantity  $\bar{\mu}$  is an approximation to the true magnetic moment, which contains all orders in expansion in the smallness parameter. Equations (9) and (10) describe nonlinear perpendicular dynamics of a particle around the cyclotron resonance. Note that exact resonances are also allowed as long as they happen locally in space and during short intervals of time. This is necessary to make sure that the increment in  $v_{\perp}$  in Eq. (10) is small (compared to  $v_{\perp}$ ) during each of these wave-particle interactions near resonances, which is the case in tokamak experiments.

Self-consistency is obtained by solving Poisson's equation

$$\nabla^2 \Phi(\mathbf{x}, t) = -4\pi \sum_s q_s \int f_s(\mathbf{x}, \mathbf{v}, t) d\mathbf{v}, \quad (11)$$

where  $f_s(\mathbf{x}, \mathbf{v}, t)$  is the distribution function in particle coordinates for species  $s$ . The density on the right-hand side is

$$\begin{aligned} \int f_s(\mathbf{x}, \mathbf{v}, t) d\mathbf{v} &= \int f_s(\bar{\mathbf{Z}}, t) \delta(\bar{\mathbf{X}} - \mathbf{x} + \boldsymbol{\rho}) d\bar{\mathbf{Z}} \\ &= \int (1 + \delta\mathbf{T}) F_s(\bar{\mathbf{Z}}, t) \delta(\bar{\mathbf{X}} - \mathbf{x} + \boldsymbol{\rho}) d\bar{\mathbf{Z}}. \end{aligned} \quad (12)$$

In the gyrocenter coordinates a near-identity transformation  $\mathbf{T}_{\text{gyro}}^* = \mathbf{1} + \delta\mathbf{T}$  divides the particle density into two parts. The first part is due to the gyrocenter distribution function  $F(\bar{\mathbf{Z}}, t)$ . The second part is the contribution due to the gyrophase dependent part of the distribution function, which describes polarization effects due to gyromotion. The unit vector  $\hat{\mathbf{b}}$  is along the ambient magnetic field.

## III. 6D NUMERICAL ALGORITHM

Low frequency gyrokinetics only solves Eq. (4) along with an appropriate gyrokinetic Poisson equation.<sup>2</sup> Instead of individual particle's trajectories, the low frequency gyrokinetics sees motion of gyrocenters with rigid uniformly charged rings attached to them (Fig. 1). The purpose of these

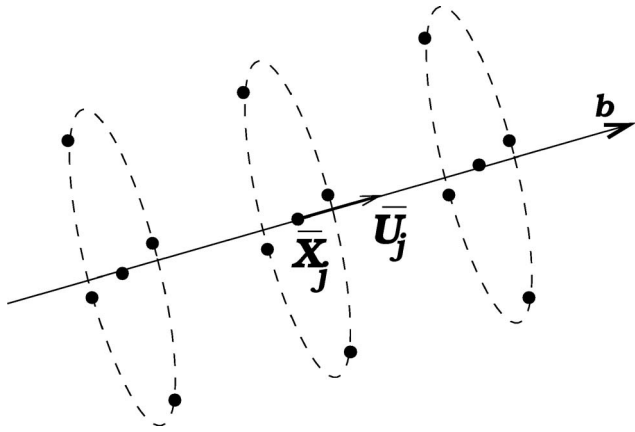


FIG. 1. Motion of a particle from the low frequency gyrokinetic point of view. Particle  $j$  has a gyrocenter located at  $\bar{X}_j$  with a parallel velocity  $\bar{U}_j$ . Each gyrocenter has a rigid charged ring attached to it.

rings is to take FLR effects into account by appropriate averaging technique via a finite number of points on each ring.<sup>10</sup>

For the arbitrary frequency case in the electrostatic limit, Eqs. (4) and (9) for the gyrocenter and gyrophase dynamics need to be solved together with Poisson's equation (11) and the conservation of the magnetic moment [Eq. (10)]. The gyrocenter dynamics described by Eq. (4) is easily simulated by a *gyrocenter pusher*,<sup>10</sup> which advances each particle's gyrocenter location  $\bar{X}$  and parallel velocity  $\bar{U}$ . Also, if  $\delta f$ -simulation<sup>16</sup> is used, then each particle will also have a gyrocenter weight  $w_j = \delta f / F|_j$  associated with it. Here  $F = F_0 + \delta f$ , with  $F_0$  being the background distribution function.

The gyrophase dependent part of the dynamics described by the equation for the generating function Eq. (9) may be simulated by a *gyrophase pusher*, which solves for functions  $g_T(\bar{Z}, t)$  and  $g_\xi(\bar{Z}, t)$ , where

$$g_T \doteq \hat{Q}_T S, \quad g_\xi \doteq \hat{Q}_\xi S. \quad (13)$$

The dynamical equations for these quantities are obtained by substituting Eq. (13) into Eq. (9).

In the arbitrary frequency regime, the motion of particles from the gyrokinetic point of view is more complicated than in the low frequency regime. Particularly, instead of individual particle's trajectories, the arbitrary frequency gyrokinetics sees the motion of gyrocenters together with *Kruskal rings*<sup>11</sup> attached to them. As before, the motion of a gyrocenter  $j$  is according to Eq. (4). The shape (the dependence of gyroradius versus gyrophase) of its Kruskal ring is determined by the rotation with the cyclotron frequency  $\dot{\xi} = \Omega(\bar{X})$ , together with conservation of the magnetic moment equation (10), which takes the following form:

$$\bar{\mu}_j(\bar{\xi}) = \frac{q}{mc} \frac{v_{\perp j}^2(\bar{\xi}, t)}{2\Omega(\bar{X})} + g_\xi(\bar{Z}_j, t), \quad (14)$$

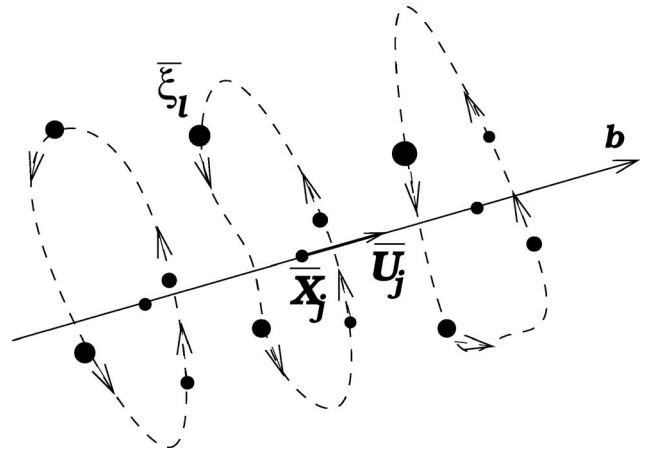


FIG. 2. Motion of a particle from the arbitrary frequency gyrokinetic point of view. Each gyrocenter ( $\bar{X}_j, \bar{U}_j$ ) has a quickly changing Kruskal ring attached to it. Finite number of ring-mates  $\bar{\xi}_l$  is simulated on each Kruskal ring. These points have different sizes to represent the amount of gyrophase weight attached to them.

$$\dot{g}_\xi(\bar{Z}_j, t) = - \frac{q^2}{\Omega(\bar{X})mc} \bar{E}_j \cdot \mathbf{v}_{\perp j}. \quad (15)$$

This Kruskal ring is quickly changing with time in a plane perpendicular to the magnetic field and is different for each particle. Appropriate gyroaveraged quantities (3) need to be calculated on Kruskal rings. Each of these Kruskal rings has a *gyrophase weight function*  $g_T(\bar{Z}_j, t)$ , which determines polarization density and evolves according to

$$\dot{g}_T(\bar{Z}_j, t) = - \left( \frac{q^2}{\Omega(\bar{X})mc} \bar{E}_j \cdot \mathbf{v}_{\perp j} \frac{\partial}{\partial \bar{\mu}_j} + \frac{q}{m} \bar{E}_j \cdot \hat{\mathbf{b}} \frac{\partial}{\partial \bar{U}_j} + \frac{q}{\Omega(\bar{X})m} \bar{E}_j \times \hat{\mathbf{b}} \cdot \frac{\partial}{\partial \bar{X}_j} \right) \ln F_0. \quad (16)$$

In a real simulation, only a finite number of points (*ring-mates*<sup>12</sup>)  $p$  on each Kruskal ring are followed (Fig. 2). For a particular gyrocenter  $j$ , we use index  $l$  to enumerate simulation ring-mates (which have the same  $\bar{X}_j$  and  $\bar{U}_j$ , but different  $\bar{\xi}_l$ 's) on its Kruskal ring. Then the dynamics of point  $l$  are determined by  $\bar{\mu}_j(\bar{\xi}_l) = \text{const}$  and the quantity  $g_T(\bar{Z}_j(\bar{\xi}_l), t)$ .

The simulation is done self-consistently by calculating Poisson's equation (11). The appropriate gyrophase integration in the density term is approximated by the summation over  $p$  ring-mates on each Kruskal ring

$$\sum_j \langle [w_j(t) + g_T(\bar{Z}_j, t)] \delta(\bar{X}_j - \mathbf{x} + \boldsymbol{\rho}_j) \rangle - \sum_j \sum_{l=1}^p [w_j(t) + g_T(\bar{Z}_j(\bar{\xi}_l), t)] \delta(\bar{X}_j - \mathbf{x} + \boldsymbol{\rho}_j(\bar{\xi}_l)). \quad (17)$$

The accuracy of this approximation is determined by the resolution of the gyrophase subspace by the total number of points  $p$  on each Kruskal ring. Particularly, for this 6D approach, the number of points  $p$  we need to keep on each

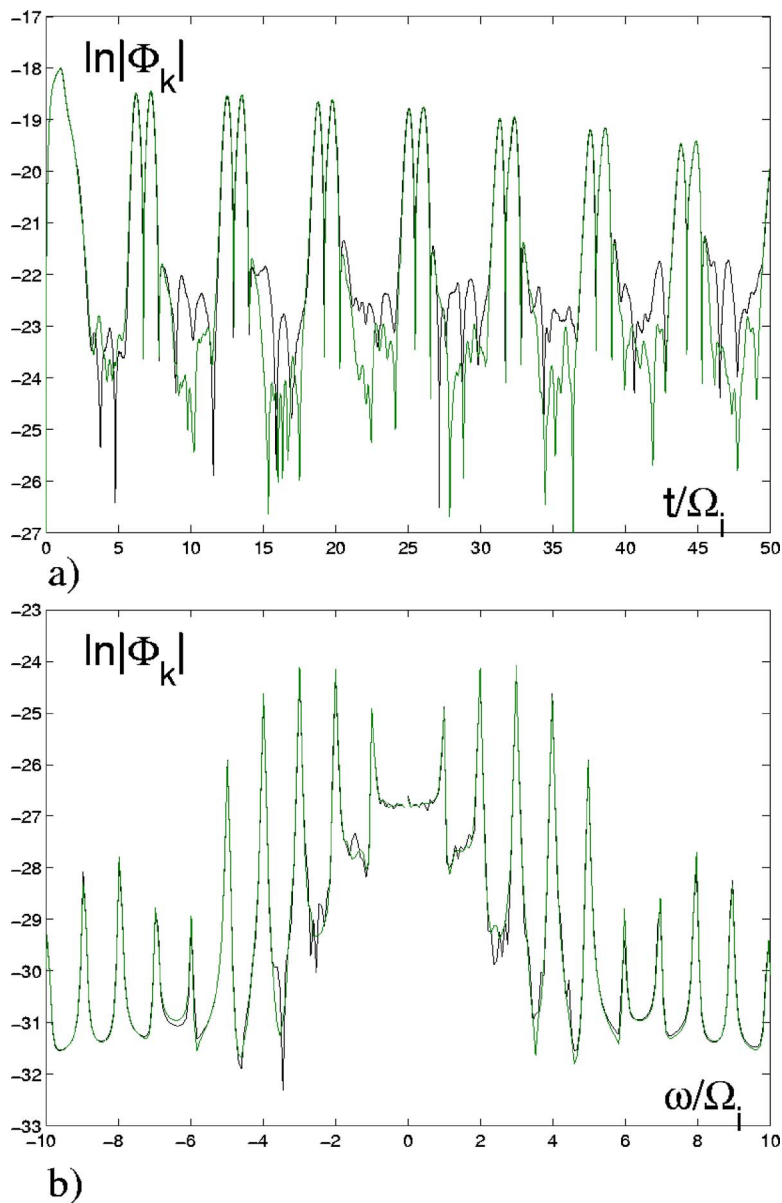


FIG. 3. (Color online) (a) Time dependencies of the amplitude of the ion Bernstein wave from 6D high-frequency gyrokinetic (black curves) and 6D Lorentz-force (green curves) codes. (b) Frequency spectra (on a logarithmic scale).

Kruskal ring for accurate estimation of averaged quantities is determined by the characteristic  $k_{\perp}\rho$  we want to study in the system.<sup>10</sup> In conventional low frequency gyrokinetics, the evolution of the Kruskal rings is present implicitly in the polarization density term of the gyrokinetic Poisson equation.<sup>2</sup>

We performed simple simulation of the ion Bernstein wave<sup>17</sup> in a  $16 \times 16$ -grid system (two spatial dimensions) to compare this 6D high frequency gyrokinetic approach with the conventional 6D Lorentz-force simulation. While the ions are gyrokinetic, the electrons are treated drift-kinetically. The parameters are  $(\omega_{pi}/\Omega_i)^2 = 1.0$ ,  $k_{\parallel}/k_y = 0.01$ . As for the initial conditions, the both ions and electrons are distributed randomly in two spatial dimensions. In the beginning  $\Omega_i t \sim 0.2$ , a constant electric field (with amplitude larger than the noise level) was applied to a system to produce waves propagating in both directions. Periodic boundary conditions were used in both spatial directions.

Figure 3 shows time dependencies and frequency spectra

of the  $k_{\perp}\rho_i = 4.4$  mode from both 6D high frequency gyrokinetic (black curves) and 6D Lorentz-force (green curves) simulations. In the first approach we used  $N_{gc} = 5000$  gyrocenters (with  $p = 16$  ring-mates on each Kruskal ring), while for the second approach we took  $N_p = 80000$  particles to make sure that the total number of simulation markers in 6D phase space is the same in both cases according to

$$N_p = pN_{gc}. \quad (18)$$

Equation (18) also makes sure that the resolution of the perpendicular (gyrophase) dynamics is the same in both cases. Both simulations produce similar results. The frequencies and damping rates of the harmonics are in agreement with the theoretical prediction from the appropriate dispersion relation.<sup>18</sup> Particularly, the predicted damping rates of the second and third harmonics are about  $(0.029 - 0.044)\Omega_i$ , which agrees with the damping rate observed in Fig. 3.

The number of differential equations solved by the 6D high frequency gyrokinetic code is  $(5+p)N_{gc}$ , while the num-

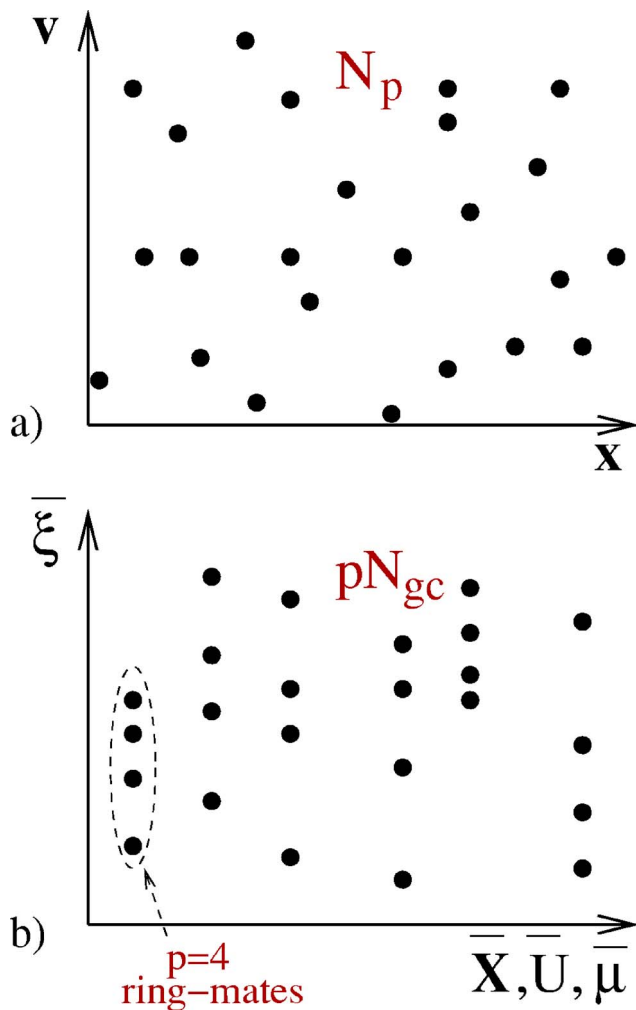


FIG. 4. (Color online) Simulation markers in 6D phase spaces. (a) 6D Lorentz-force simulation with  $N_p$  particles sampling  $(x, v)$  space. (b) 6D high frequency gyrokinetic simulation with  $N_{gc}$  gyrocenters (each has  $p=4$  ring-mates) sampling  $\bar{Z}$  space.

ber of equations solved by the 6D Lorentz-force code is  $6N_p$ . Using the constraint (18), we estimate that the former approach is  $6p/(5+p)$  times faster than the latter one. The Lorentz-force code takes a larger amount of computing time (more differential equations are solved) since particles participate in resolution of all 6D phase space, while points on Kruskal rings in the gyrokinetic code only resolve 1D gyrophase subspace. The remaining 5D gyrocenter subspace is resolved by the total number of gyrocenters in the simulation (Fig. 4). The separation of motions introduced by the gyrokinetic formalism always makes sure that the motion of gyrocenters is slow compared to the gyrophase dynamics. The decoupled 5D gyrocenter dynamics needs to be simulated by the regular low-frequency gyrokinetic equation (4) which normally requires fewer simulation gyrocenters due to lower dimensionality and slow dynamics.<sup>2</sup> Numerically, one needs to choose the number of gyrocenters  $N_{gc}$  and push them with large time step  $\Delta T$  determined by the microinstability time scales. Then one chooses the number of ring-mates  $p$  to put more resolution into the gyrophase which needs to be treated with smaller step  $\Delta t$  determined by the highest cyclotron

harmonic in the simulation. This ability of the new algorithm to redistribute numerical resources in accordance with different needs in resolution and time steps is what allows this approach to be up to six times faster than the direct Lorentz-force simulation. Separation of microinstability and cyclotron time scales makes new 6D high frequency gyrokinetic algorithm suitable for implementation into existing gyrokinetic codes.<sup>9</sup>

In the example in Fig. 3 we had  $\Delta T = 10\Delta t = 0.1/\Omega_i$  in our new gyrokinetic simulation, while only small time step  $\Delta t$  was used in the Lorentz-force code. This resulted in about 40% saving of computing time in our 6D high frequency gyrokinetic code compared to the 6D Lorentz-force code.

Although this example is simple, our new algorithm may be straightforwardly applied to systems with complicated geometries and inhomogeneities like tokamak plasmas. The amount of saving in computing time due to pushing gyrocenters with larger time step will depend on the amount of time a particular code spends on gyrocenters. Since this is usually the most time consuming part in particle codes, utilizing the 6D high frequency algorithm instead of the direct Lorentz-force approach may result in significant saving in computing time. This new algorithm also allows enough flexibility to analytically transform the gyrophase dynamics into a set of equations for individual harmonics, which, in certain situations, may result in further saving in computing time. This will be considered in the next section.

In a previous computational example we only considered linear dynamics of the ion Bernstein wave. Within the 6D high frequency gyrokinetic algorithm, fast nonlinear dynamics is captured by the evolution of Kruskal rings' shapes (dependence of gyroradius on gyrophase) according to the conservation of the magnetic moment equation (14) for each ring-mate. Quickly changing Kruskal rings' shapes are then used to find electric fields at ring-mates' positions to calculate the gyrophase weight function equation (16). As a result, one recovers nonlinear effects, particularly, stochastic ion heating<sup>19</sup> and wave coupling. Also, various gyrophase-averaged quantities necessary for gyrocenter dynamics (4) and densities in Poisson's equation (17) need to be calculated by appropriate averaging on Kruskal rings.

#### IV. 5D NUMERICAL ALGORITHM

In the limit of small gyroradius  $\rho/L_B \ll 1$ , the 6D approach described above is equivalent to the integration of electrostatic Lorentz-force equations along particle orbits. The advantage brought by the high frequency gyrokinetics is twofold. First, as mentioned before, a larger time step for pushing gyrocenters may be used, which saves computing time. Second, as opposed to the 6D Lorentz force simulation, the explicit gyrophase dependence may be removed from the algorithm. Particularly, this transformation may be performed by rewriting the original functions  $g_T(\bar{Z}, t)$  and  $g_\xi(\bar{Z}, t)$  as follows:<sup>7</sup>

$$g(\bar{\mathbf{Z}}, t) = \sum_{n=-\infty}^{n=\infty} g_n(\bar{\mathbf{X}}, \bar{\mathbf{U}}, \bar{\boldsymbol{\mu}}, t) e^{in\bar{\xi}}. \quad (19)$$

Complex functions  $g_n$ , resulting from the Fourier transform in gyrophase subspace, are 5D and they separately describe the dynamics of different harmonics. The dynamical equation for harmonic  $n$  is obtained by substituting Eq. (19) into Eq. (13). Particularly, one obtains

$$\left( \frac{d}{dt} + in\Omega(\bar{\mathbf{X}}) \right) g_n = q \langle \hat{\mathbf{Q}} \tilde{\Phi}(\bar{\mathbf{X}} + \boldsymbol{\rho}, t) e^{-in\bar{\xi}} \rangle, \quad (20)$$

while the polarization density equation (17) may be rewritten as follows:

$$\sum_j \left\langle \sum_{n=-\infty}^{n=\infty} g_{Tn}(\bar{\mathbf{X}}_j, \bar{\mathbf{U}}_j, \bar{\boldsymbol{\mu}}_j, t) e^{in\bar{\xi}} \delta(\bar{\mathbf{X}}_j - \mathbf{x} + \boldsymbol{\rho}_j) \right\rangle. \quad (21)$$

The gyrophase-dependent information is efficiently described by the finite number of harmonics kept in the system. Essentially, we Fourier transform (in the gyrophase variable) the complicated shapes of Kruskal rings and keep the harmonics which contribute the most. Now both parallel distribution  $F$  and gauge  $g_n$  functions are the functions in 5D phase space  $(\bar{\mathbf{X}}, \bar{\mathbf{U}}, \bar{\boldsymbol{\mu}})$ . Note that this transformation from the original 6D to 5D algorithm is not a reduction in dimensionality procedure like in obtaining the drift-kinetic equation when part of the dynamics is averaged away. In the 5D algorithm, instead, the high frequency part is still present in the form of a set of equations for individual harmonics. The name ‘‘5D’’ for this approach is chosen to emphasize that the dynamical functions  $F$  and  $g_n$  do not explicitly depend on gyrophase.

To take advantage of this 5D approach, the integrals in Eqs. (20) and (21) need to be estimated analytically either in  $\mathbf{k}$  or real space. As opposed to the 6D simulation, the 5D high frequency gyrokinetic algorithm does not require us to solve separate differential equations for each ring-mate on its Kruskal ring. Particularly, as was mentioned before in Sec. III, the code based on the 6D algorithm solves  $(5+p)N_{\text{gc}}$  differential equations (and  $p$  may be sufficiently large). The code based on the 5D high frequency gyrokinetic algorithm would need to solve  $(5+2m)N_{\text{gc}}$  equations, where  $m$  is the number of harmonics kept in the system. The number of harmonics one needs to keep depends on the problem under consideration. Both the 6D and 5D algorithm take approximately the same amount of computing time if

$$p = 2m. \quad (22)$$

If  $p > 2m$ , the 5D simulation may take less computing time than the direct 6D simulation. Note that the relation (22) is not an antialiasing condition; it compares numerical efficiency of algorithms.

Here we again use an example of the ion Bernstein wave  $[(\omega_{pi}/\Omega_i)^2 = 1.0, k_{\parallel}/k_y = 0.01]$  to illustrate the difference between 6D and 5D high frequency gyrokinetic algorithms. Figure 5 shows the time dependencies and the frequency spectra of the  $k_{\perp}\rho_i = 4.4$  mode from both 6D (black curves) and 5D high frequency gyrokinetic (red curves) simulations.

In both cases  $N_{\text{gc}} = 5000$  gyrocenters were used. As before, in the 6D algorithm we took  $p = 16$  points on each Kruskal ring. In the 5D algorithm only three harmonics ( $n = \pm 2, \pm 3, \pm 4$ ) with the largest amplitudes were kept ( $m = 3$ ). Appropriate expressions in  $\mathbf{k}$  space were used instead of gyrophase integrals Eqs. (20) and (21). Particularly, the polarization density equation (21) may be rewritten as follows:

$$\sum_j \sum_{n=-\infty}^{n=\infty} a_n \delta(\bar{\mathbf{X}}_j - \mathbf{x}), \quad (23)$$

with the quantity  $a_n(\bar{\mathbf{X}}_j, \bar{\mathbf{U}}_j, \bar{\boldsymbol{\mu}}_j, t)$  evolving according to

$$\left( \frac{d}{dt} + in\Omega(\bar{\mathbf{X}}_j) \right) a_n = \sum_{\mathbf{k}} J_n^2(k_{\perp}\rho_j) \alpha_{\mathbf{k}} e^{-ik \cdot \bar{\mathbf{X}}_j}, \quad (24)$$

where

$$\alpha_{\mathbf{k}} = -2\pi \left( in \frac{q^2}{mc} \Phi_{\mathbf{k}} - U_j(\mathbf{b} \cdot \mathbf{E})_{\mathbf{k}} \right). \quad (25)$$

The right-hand side of Eq. (24) is calculated only for a finite number of  $\rho$ 's at each time step to approximate the behavior of the Bessel function. For each particle this right-hand side is determined from interpolation of obtained data according to its  $\rho$ . Figure 5 shows that the dynamics of the chosen harmonics is described appropriately (including electron Landau damping), with the rest of the harmonics being excluded from the picture. In this example the 5D high frequency gyrokinetic algorithm solves approximately twice as few differential equations (and takes about 50% of computing time) compared to the 6D algorithm.

The initial conditions in Fig. 5 are the same as in the previous example. In spite of the fact that there are all possible harmonics contained in the initial seed electric field, the 5D algorithm extracts only the information about the harmonics we choose. This is the reason why there is only a finite number of harmonics in the frequency spectrum for a particular mode.

Note that if we choose to interpolate the integrals in Eqs. (20) and (21) in  $\mathbf{k}$  space as done in previous example, the smallest  $\mathbf{k}$  in the system must be anticipated in the gridding. This may be done by performing local Fourier transform in the mode conversion regions where large  $\mathbf{k}$  modes are present.

As before, this computational example was used to study linear dynamics. To include nonlinear dynamics into the 5D high frequency gyrokinetic algorithm, one must obtain appropriate analytical expressions for gyrophase-averaged quantities (3). For example, in  $\mathbf{k}$  space the right-hand side of Eq. (20) may be rewritten as follows:

$$\begin{aligned} & \langle \hat{\mathbf{Q}} \tilde{\Phi}(\bar{\mathbf{X}} + \boldsymbol{\rho}, t) e^{-in\bar{\xi}} \rangle \\ & \approx \hat{\mathbf{Q}} \tilde{\Phi}(\bar{\mathbf{X}}, t) \left( I_n(ik_{\perp}\rho_0) - \sum_m \frac{ik_{\perp}\rho_0}{2\bar{\boldsymbol{\mu}}} I'_m(ik_{\perp}\rho_0) g_{m-n} \right). \end{aligned} \quad (26)$$

Here  $\rho_0 = \sqrt{2c\bar{\boldsymbol{\mu}}/e\Omega}$  is the particle's gyroradius in the beginning of the simulation. The first term in the right-hand side of Eq. (26) is the linear contribution, while the second term

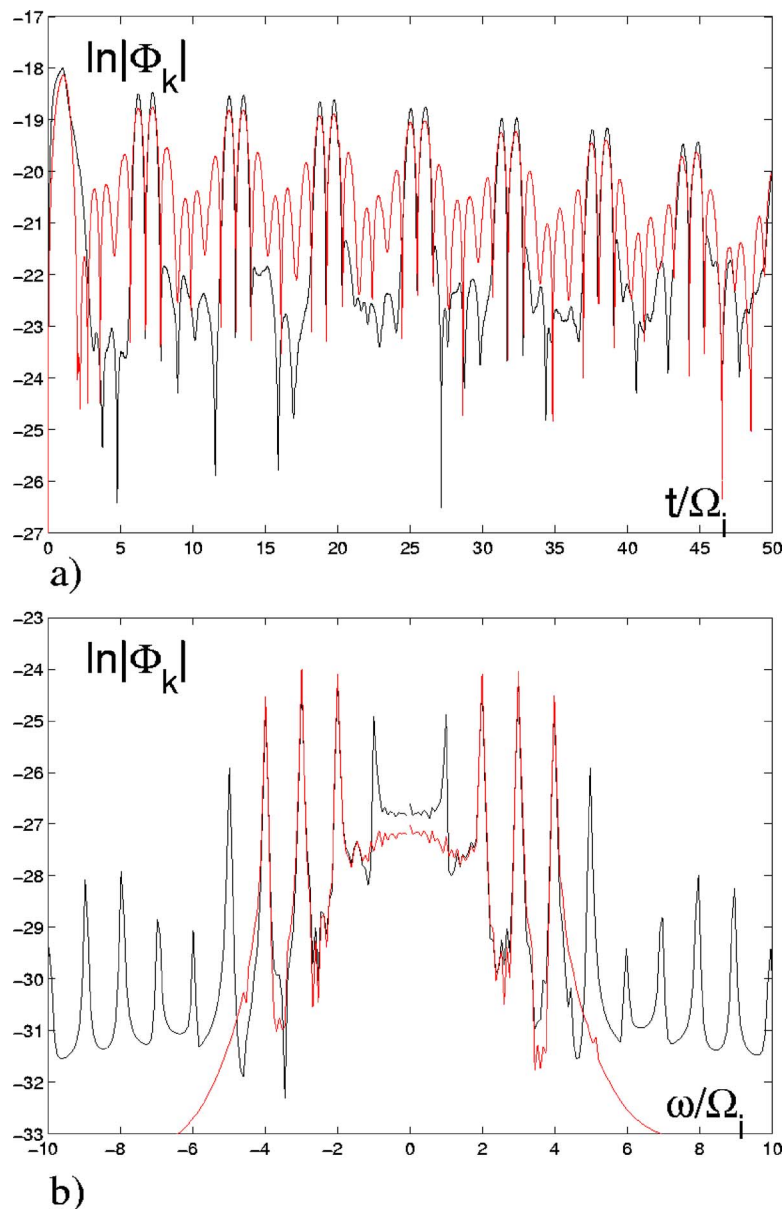


FIG. 5. (Color online) (a) Time dependencies of the amplitude of the ion Bernstein wave from the 6D (black curves) and 5D high frequency gyrokinetic (red curves) codes. (b) Frequency spectra (on a logarithmic scale).

gives nonlinear dynamics of three-wave coupling between harmonics  $n$ ,  $m$ , and  $p$  satisfy  $p=m-n$ . It may be that the choice of important harmonics is not clear. If this is the case, one cannot effectively utilize the 5D algorithm to study the dynamics of parametric decay. Efficient ways to treat fast nonlinearities in the 5D algorithm with no loss of gyrophase information is a subject of future research.

## V. DISCUSSION AND FUTURE WORK

The high frequency gyrokinetic algorithm may be readily generalized to electromagnetic systems, which is a subject for future research. The new 6D and 5D versions of the algorithm may be especially useful for computational study of the dynamics of propagation, conversion, and absorption of radio frequency waves in tokamak plasmas. Some of the approaches utilized for studying the wave-plasma interaction include combination of wave solvers<sup>13</sup> with Fokker-Planck codes<sup>14</sup> and Monte Carlo simulation.<sup>15</sup> These approaches assume heating dynamics to be quasilinear

which can be approximated by the diffusion in velocity space. While quasilinear theory may be a good approximation in the electron cyclotron heating case, it can be argued that it breaks down for ion interactions.<sup>15</sup> Our new approach describes the nonlinear heating dynamics based on first principles physics. In gyrokinetic formulation the perpendicular heating dynamics is completely described by the evolution of shapes of the Kruskal rings according to conservation of magnetic moment equation (10). Equations (9) and (10) allow for both regular and secular solutions, which produce the heating rate. Similar to a direct Lorentz-force simulation,<sup>5</sup> the new approach presented in this paper can self-consistently describe the wave dynamics together with the evolution of non-Maxwellian parts of distribution functions, particle orbits, etc. Also, it allows us to address the issue of interaction between wave dynamics and microinstability-driven turbulence.

Since the electromagnetic wave propagating in inhomogeneous plasma can go through mode conversion layers

where perpendicular wavenumber  $k_{\perp}\rho_i$  may become large, connecting 6D and 5D algorithms into one global code can result in further saving in computing time. For example, in the regions of sufficiently long perpendicular wavelengths  $k_{\perp}\rho_i \approx 1.0$ , one can simulate  $p \approx 4$  ring-mates on Kruskal rings with the 6D algorithm. In the regions where the dynamics of short wavelengths  $k_{\perp}\rho_i \gg 1.0$  is important (for example, determined from local Fourier transform of the mode structure), correct simulation of the 6D algorithm would require too many ring-mates. Hence, the 5D algorithm may be an optimal approach to treat these regions.

In summary, a high frequency gyrokinetic particle-in-cell algorithm was developed, which allows one to simulate electrostatic arbitrary frequency and wavelength physics for  $\rho/L_B \ll 1$  and  $e\Phi/T \ll 1$ . This algorithm is based on the gyrocenter-gauge kinetic theory,<sup>6</sup> which transforms the original Vlasov equation to the system of decoupled equations for the gyrocenter distribution  $F(\bar{X}, \bar{U}, \bar{\mu}, t)$  and gauge  $S(\bar{Z}, t)$  functions. The high frequency gyrokinetics describes each particle as a combination of a gyrocenter and a complicated, quickly changing Kruskal ring. The new 6D algorithm allows a self-consistent simulation of nonlinear interaction between electrostatic waves and plasma, based on first principle physics. The gyrokinetics naturally separates gyrophase and gyrocenter dynamics. This allows us to use larger time steps to treat slower gyrocenter motion and thus saves on computing time compared to the 6D Lorentz-force simulation. Also, explicit dependence on the gyrophase variable may be removed from the 6D algorithm. In the resulting 5D algorithm the gyrophase dynamics is transformed into a set of equations for a finite number of harmonics. In special situations this can result in further computing time saving. In future publications, we will describe the electromagnetic ver-

sion of the algorithm to address the physics of propagation, conversion, and absorption of radio frequency waves launched by an antenna. Our ultimate interest is to use this algorithm to perform global gyrokinetic simulation of experimentally relevant wave heating dynamics in fusion devices.

## ACKNOWLEDGMENTS

This work was supported by the Multi-Scale Gyrokinetics project as a part of the U.S. DOE ASCR Multiscale Mathematics Research and Education Program.

- <sup>1</sup>R. G. Littlejohn, Phys. Fluids **24**, 1730 (1981).
- <sup>2</sup>W. W. Lee, Phys. Fluids **26**, 556 (1983).
- <sup>3</sup>T. S. Hahm, Phys. Fluids **31**, 2670 (1988).
- <sup>4</sup>D. H. E. Dubin, J. A. Krommes, C. Oberman, and W. W. Lee, Phys. Fluids **26**, 3524 (1983).
- <sup>5</sup>V. K. Decyk, and H. Abe, Phys. Fluids **29**, 559 (1986).
- <sup>6</sup>H. Qin, W. M. Tang, W. W. Lee, and G. Rewoldt, Phys. Plasmas **6**, 1575 (1999).
- <sup>7</sup>H. Qin, W. M. Tang, and W. W. Lee, Phys. Plasmas **7**, 4433 (2000).
- <sup>8</sup>X. S. Lee, J. R. Myra, and P. J. Catto, Phys. Fluids **26**, 223 (1983).
- <sup>9</sup>Z. Lin, T. S. Hahm, W. W. Lee, W. M. Tang, and R. B. White, Science **281**, 1835 (1998).
- <sup>10</sup>W. W. Lee, J. Comput. Phys. **72**, 243 (1987).
- <sup>11</sup>H. Qin, Fields Inst. Commun. **46**, 171 (2005).
- <sup>12</sup>M. Kruskal, J. Math. Phys. **3**, 806 (1962).
- <sup>13</sup>E. F. Jaeger, L. A. Berry, J. R. Myra *et al.*, Phys. Rev. Lett. **90**, 195001 (2003).
- <sup>14</sup>R. W. Harvey, O. Sauter, R. Prater, A. P. Nikkola *et al.*, Phys. Rev. Lett. **88**, 205001 (2002).
- <sup>15</sup>M. Choi, V. S. Chan, R. I. Pinsker, S. C. Chiu, and W. W. Heidbrink, Phys. Plasmas **12**, 072505 (2005).
- <sup>16</sup>S. E. Parker and W. W. Lee, Phys. Fluids B **5**, 77 (1993).
- <sup>17</sup>M. Ono, Phys. Fluids B **5**, 241 (1993).
- <sup>18</sup>T. H. Stix, *Waves in Plasmas* (American Institute of Physics, New York, 1992).
- <sup>19</sup>R. A. Kolesnikov, W. W. Lee, H. Qin, and E. Startsev, *17th Topical Conference on Radio Frequency Power in Plasmas, Clearwater, FL, 2007* (American Institute of Physics, Melville, NY, in press).